A New Structure Optimization Method for the Interneedle Distance of a Multineedle-to-Plane Barrier Discharge Reactor

Mingzhe Rong, *Member, IEEE*, Dingxin Liu, Dong Wang, Biao Su, Xiaohua Wang, and Yi Wu

***Abstract*—A new method for the interneedle-distance optimization of a multineedle-to-plane barrier discharge reactor is presented. As we know, there is gas breakdown when, in some regions between electrodes, the electric field is higher than the breakdown field; hence, the region may play a dominant role for the discharge, and the enhancement of its volume ratio in the reactor will allow an increase in discharge energy density. This can be achieved by structure optimization. With the finite-element method, the 3-D profiles of an electrostatic field in the reactor are acquired for a series of interneedle distances, thereby the one-to-one relationship between the volume ratio and interneedle distance is obtained. This allows the optimal interneedle distance for power input efficiency to be identified, as related to the maximal volume ratio. The optimal distance is between 7.2 and 8.4 mm in our simulation range, decreasing with the increase of operating voltages from 16 to 26 kV. The simulation results are experimentally validated by discharge energy measurement as well as the performance of SO_2 removal from indoor air. This structure optimization method leads to a simple way to obtain the optimal interneedle distance for energy input efficiency and hence benefits commercial use.**

***Index Terms*—Dielectric barrier discharge (DBD), electrostatic field simulation, energy efficiency, structure optimization.**

I. Introduction

DIELECTRIC barrier discharges (DBDs) provide a simple technology to establish a nonthermal plasma condition in atmospheric air. This property has led to a number of industrial applications, such as ozone generation, surface modification, air pollution control, etc. [1]. Generally, plane-parallel or coaxial geometries are adopted for DBD electrodes, but the multineedle-to-plane (MP) structure is proven to be better for some applications, such as air pollution control. Compared with plane-parallel or coaxial geometries, the use of MP geometry has several advantages, such as low operating voltage, low dielectric loss, and high toxic gas removal yield, which are, again, beneficial for commercial use [2].

Manuscript received November 5, 2009; revised January 26, 2010. First published March 18, 2010; current version published April 9, 2010. This work was supported in part by the National Natural Science Foundation of China under Grants 50525722 and 50907053 and in part by the Basic Research Fund of State Key Laboratory of Electrical Insulation and Power Equipment.

The authors are with the State Key Laboratory of Electrical Insulation and Power Equipment, and also with School of Electrical Engineering, Xi'an Jiaotong University, Xi'an 710049, China (e-mail: mzrong@mail.xjtu.edu.cn; liudingxin@gmail.com; wangdong@stu.xjtu.edu.cn; subiao@stu.xjtu.edu.cn; xhw@mail.xjtu.edu.cn; wuyic51@mail.xjtu.edu.cn).

Color versions of one or more of the figures in this paper are available online at http://ieeexplore.ieee.org.

Digital Object Identifier 10.1109/TPS.2010.2042733

An MP structure usually consists of an electrode with several arrays of needles and a plane electrode covered by a dielectric barrier [3], [4]. Therefore, the performance of an MP barrier discharge has many structural influencing factors, e.g., interneedle distance, the gap between needle and plane electrode, the needles' shape, and so on. In order to improve applications of MP geometry, many efforts have been made on structure optimization, but mainly through comparative experiments [3]–[6]. A great deal of work is required for this method, but the results are only valid for a limited number of cases. Therefore, a new method based on the fundamental law that can be used much more widely is required.

For some applications, such as air pollution control, performance is a strong function of power input over gas flow rate [7]. It is commercially required to enhance the energy input efficiency by the structure optimization of the reactor. To this end, the 3-D finite-element method (FEM) is utilized in this study, and the profiles of electrostatic field are acquired for a series of interneedle distances and operating voltages. As we know, avalanches are generated in the region in which electric field $E > 26$ kV/cm in atmospheric air [8]; hence, such region is termed the active region (AR) in this paper. The AR may play a dominant role for discharge intensity, and hence, the increase of its volume ratio in the reactor (the volume of AR over the entire air volume between the MP electrodes) may result in higher energy input efficiency. By electrostatic simulation, the relationship between the interneedle distance and volume ratio of AR is identified. Therefore, the optimal interneedle distance corresponding to the maximal volume ratio can be found out as a function of operating voltage.

In our simulation range, the interneedle distance of 2–20 mm is taken into account, and the optimal distance is found to decrease from 8.4 to 7.2 mm as the operating voltage increases from 16 to 26 kV. Also, if we plot the interneedle distance and operating voltage into one figure, a relatively large band exists, in which the volume ratio of AR is more than 99% of the biggest ones, which means that the interneedle distance in this band should always be good. We defined the band to be valid band (VB) in this paper. The width of VB is 1.2 mm, which is large enough for a roughly chosen interneedle distance for commercial use. All the simulation results are validated by discharge energy measurement as well as SO_2 removal experiments.

The structure optimization method could be applied to other structural influencing factors of the MP barrier discharge, even

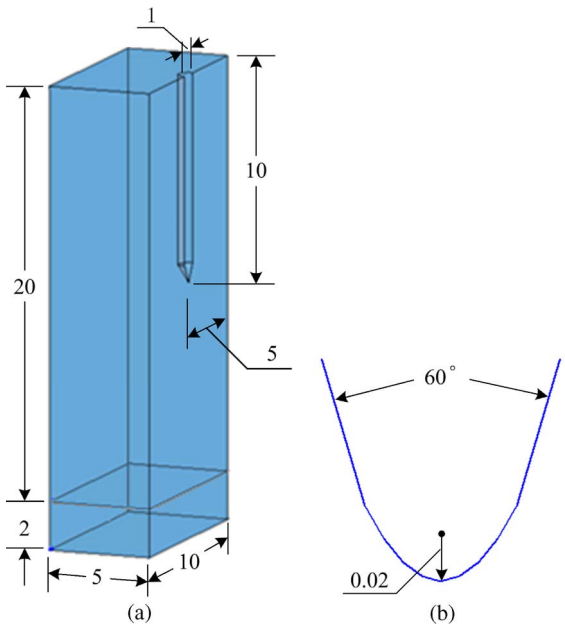

Fig. 1. Simulation model of MP geometry (unit in millimeters). (a) MP geometry in the case of a 10-mm interneedle distance. (b) Schematic diagram of the tip of the needle.

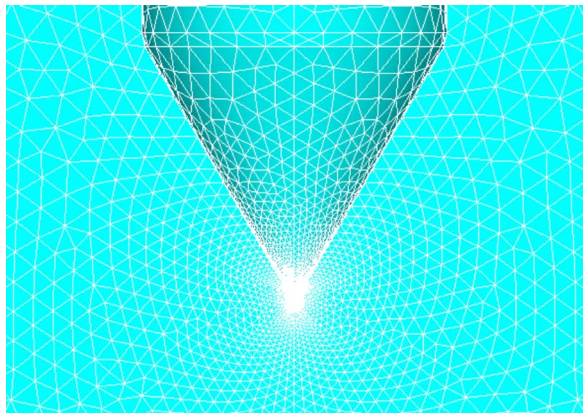

Fig. 2. Zoom view of the local mesh around the needle end.

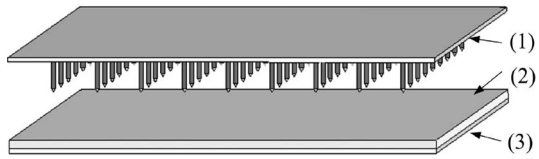

Fig. 3. Schematic diagram of MP electrodes. (1) Multineedle electrode. (2) Dielectric barrier. (3) Plane electrode.

for other types of discharge such as corona discharge. However, it is better for this method to be limited in low-frequency and low-power-density discharges, because the eigenfield and memory effect in high-frequency plasmas are so strong that electrostatic simulation may suffer intolerable error [9].

II. Model

In recent years, computational modeling in the electrostatic field has been widely utilized with the advent of powerful computers. It is adopted here to get the optimal interneedle distance for MP barrier discharges, too. Compared with other kinds of models, such as a fluid model, this model is obviously much easier and time saving. Although it is not so accurate, it is effective for the structure optimization of low-frequency and low-power-density discharges, which can be experimentally validated later.

The calculation is realized by solving the electrostatic Laplace equation with a well-known FEM software named ANSYS. As shown in Fig. 1, the 3-D model is a half model since, in this case, the electric field is symmetrical. It is noted that a 1/4 model could also be used because of the symmetry of the electric field, and hence, it would save more computational resources. However, a half model is adopted for the sake of making the figures more intuitionistic. The power is applied to upper and needle surfaces, with the bottom surface grounded. No external circuit is included. A large scale of operating voltage from 16 to 26 kV with a resolution of 1 kV is investigated. All the side faces are set to be plane symmetrical, for there is no voltage gradient on these boundaries due to the mutual effect of needles nearby.

For simplification, the structural parameters are unchangeable except for the interneedle distance, which is from 2 to 20 mm with a resolution of 0.5 mm in simulation. The gap between the needle and the dielectric board is 10 mm [Fig. 1(a)]. The board is 2 mm thick, and its relative dielectric constant is 2.2. The shape of each needle is the same as a cylinder of 1-mm diameter and 10-mm length with a cone end of 60° angle. At the tip, the curvature radius is 20 μm [Fig. 1(b)]. Nearly all the parameters in the model are similar to the actual reactor, except for the resolution of interneedle distance. The resolution is 2.5 mm in the actual reactor rather than 0.5 mm in the simulation, due to the manufacturing restriction.

Tetrahedral cells with ten nodes each are used for the mesh, as shown in Fig. 2. The electric field changes rapidly near the needle's tip, so that the simulation result is quite sensitive to the mesh resolution in this region, which is also found in [10] when modeling an RF plasma needle with FEM. The mesh size near the needle tip is set to be 2 μm in this study, and the total number of cells for each case is between 150 000 and 300 000, differing with different distances. It is noted that, near the needle tip, we have tried a smaller mesh size like 1 μm; however, the simulation shows similar results. This indicates that the meshes are fine enough to capture the electrostatic field in this study.

In order to identify AR and VB, as well as to get the volume ratio of AR as a function of interneedle distance and operating voltage, the postprocessing of ANSYS is utilized in combination with MATLAB for the final stage of analysis.

III. Experimental Setup

The schematic diagram of the MP geometry used for experiments is shown in Fig. 3. It contains two plane electrodes of 100 × 100 mm. Several arrays of needles are fitted on the upper electrode. Either needle can be detached from the plane electrode; hence, it is convenient to change the interneedle distance. All the geometry parameters have been described in

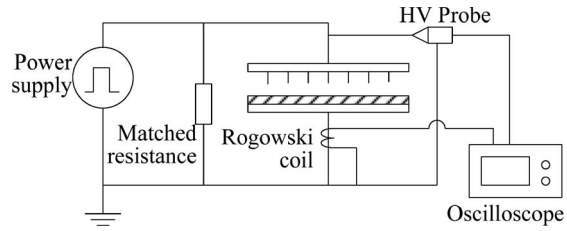

Fig. 4. Electrical system in the experimental setup.

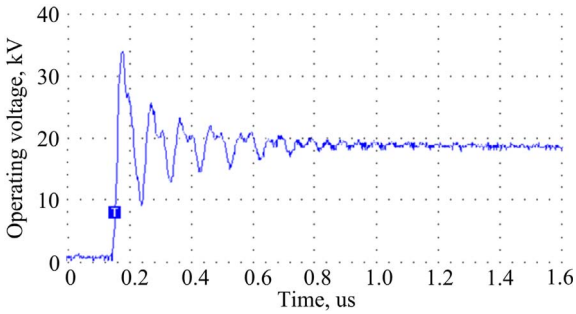

Fig. 5. Rising part of the pulsed voltage.

Section II. The dielectric board is made of epoxy resin ($\varepsilon_r = 2.2$), and the others are made of copper.

Pulsed voltage is applied on the needle electrode, as shown in Fig. 4. The power supply is developed by Dalian University of Technology, China. A spark switch is used for unipolar pulse generation with a frequency of 100 Hz. The operating voltage is measured using a Tektronix P6015 probe. The discharge current is measured using a Rogowski coil (Pearson 2878). The discharge energy per voltage pulse is obtained by the time integration of current and voltage. For a specific operating voltage, the interneedle distance related to the maximal energy is considered to be optimal for power input efficiency.

The pulse has a rising time of about 14 ns, and its full width at half maximum is about 1 ms. As shown in Fig. 5, the voltage is oscillating as the front part of each pulse. In this paper, the operating voltage is considered to be the average voltage of each pulse.

In order to validate the simulation results, the discharge images for a number of interneedle distances are taken by a Panasonic LX1 camera. Because discharge trajectory is changeable, which may be attributed to surface charge accumulation and interaction between nearby needles (not discussed in this paper), the exposure time is set to be 8 s, which is long enough to make sure that the images are bright and stable and, hence, easy to analyze.

Furthermore, the reactor is utilized for SO_2 removal from indoor air, and its performance is compared for different interneedle distances. The experimental facility for indoor air purification is shown in Fig. 6, similar to [11]. As shown in Fig. 6, the reaction chamber is an air-proof glass box with dimensions of 1.5 m × 1.5 m × 0.6 m(width × length × height). The flow meter is controlled by a computer to define the initial concentration of gaseous SO_2 in the chamber. A fan is used to circulate the gas through the plasma region. The gas analyzer (produced by Shijiazhuang Dynamic Instrument Industry Company Ltd.) has a sensitivity of 0.2 mg/m^3, and its time response is 30 s.

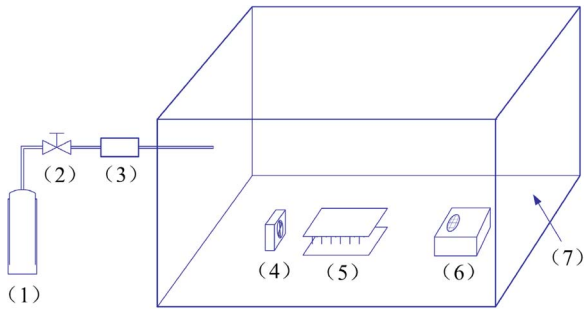

Fig. 6. Schematic diagram of the indoor air purification experimental facility. (1) SO_2 gas container. (2) Pressure-relief valve. (3) Flow meter. (4) Fan. (5) MP barrier discharge reactor. (6) Gas analyzer. (7) Glass box.

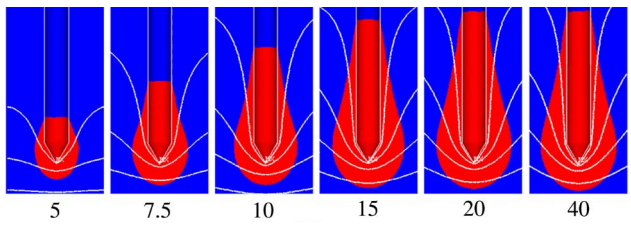

Fig. 7. Patterns of AR and potential isolines for different interneedle distances (unit is in millimeters).

The measurement results are automatically recorded by a computer. For a specific operating voltage, the same concentration (20 mg/m^3) of SO_2 is initialized, and then, the pulsed voltage is applied for 10 min. The removal mass of SO_2 is compared for different interneedle distances. As recommend by [7], the less time used, the higher the power and, hence, the higher the power input efficiency of the structure.

IV. Mutual Effect of Nearby Needles

The patterns of AR and potential isolines derived by ANSYS are shown in Fig. 7, in which the operating voltage is 20 kV and interneedle distance varies from 5 to 40 mm. It can be seen that the volume of AR (red zone) is expanding along with interneedle distance increases, but the expansion tends to be weaker as distance becomes larger, particularly when distance is larger than 20 mm. The potential curves have 2 kV of intervals. Similar to that of AR, the camber of the potential isoline increases with the interneedle distance, but when distance is larger than 20 mm, the increase is generally ceased. This means that the interaction of nearby needles can play a large role when the interneedle distance is shorter than 20 mm. As aforementioned, the expansion of AR leads to an increase of discharge intensity. Therefore, the discharge energy input per needle should increase with the interneedle distance, but the growth rate should slow down.

Assuming that the discharge energy is a positive function of light emission intensity [12], the deduction of Fig. 7 could be validated intuitively by the discharge images (see Fig. 8). For a large range of operating voltage, the dependence of discharge energy per needle on interneedle distance is similar. That is, the discharge energy (luminosity) per needle increases with the enlargement of distance, but the growth rate slows down. This attributes to the mutual effect of nearby needles. When

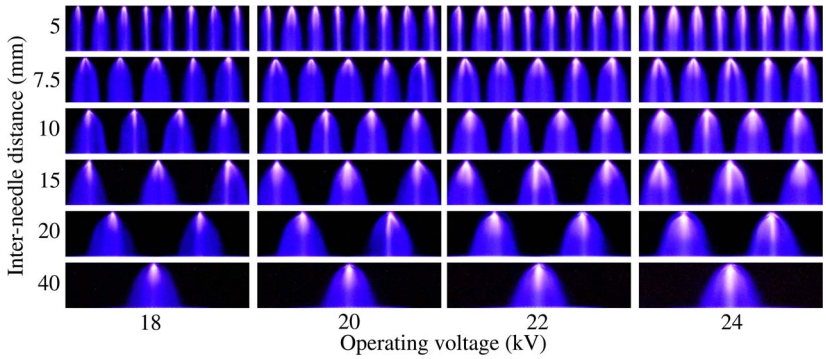

Fig. 8. Images of MP barrier discharges for different interneedle distances and operating voltages.

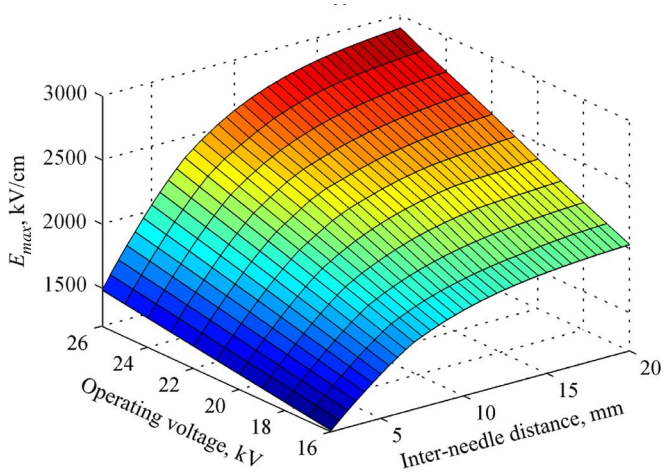

Fig. 9. $E_{\max}$ obtained by ANSYS as a function of operating voltage and interneedle distance.

the distance between two needles is small, such as 10 mm, the electric field generated by one needle could have a strong effect to the other; therefore, the total electric field gets to be more uniform that the coronalike character is weakened (see the potential isolines in Fig. 7). Therefore, the AR volume per needle gets to be smaller and discharge intensity is reduced. This mutual effect is stronger when the interneedle distance is shorter.

The mutual effect of nearby needles could be further explained by analyzing the electric field intensity at the needle's tip. Since electric field intensity reaches its maximum at the needle's tip, it is named $E_{\max}$ in this paper. As shown in Fig. 9, for a specific operating voltage, the $E_{\max}$ increases along with the enlargement of the interneedle distance, but the growth rate slows down. It is interesting that the tendency of $E_{\max}$ is similar to the expansion of the AR per needle (see Fig. 7). Therefore, it further confirms that the mutual effect of nearby needles promotes electric field uniformity, reduces the volume of AR, and hence reduces discharge intensity per needle.

It is worth mentioning that $E_{\max}$ can be calculated by an analytic formula as follows [8], when there is just one needle or when the interneedle distance is large enough (mutual effect of nearby needles is negligible)

$$E = \frac{2V}{(r+2x)\ln\frac{r+2d}{r}} \tag{1}$$

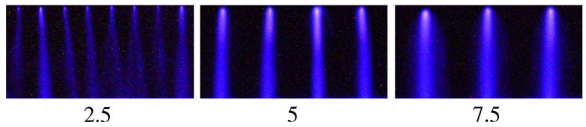

Fig. 10. Images of MP barrier discharge with short interneedle distances (unit in millimeters).

where

- E electric field intensity (in kilovolts per centimeter);
- V gap voltage (in kilovolts);
- r curvature radius at the tip of the needle (in centimeters);
- x distance to the tip of the needle (in centimeters);
- d gap between the needle's tip and plane electrodes (in centimeters).

Equation (1) can be used to check the accuracy of the FEM simulation in this paper. When no mutual effect of the nearby needles is considered, i.e., an infinite boundary condition is used for side faces instead of a plane symmetrical boundary condition (see Section II), $E_{\max} \approx 2380$ kV/cm when the operating voltage is 20 kV. This is similar to the analytic result, with only 500 kV/cm less. It is noted that (1) is for a needle with a rounded tip, which is slightly different to that modeled in this paper, and hence, the difference is reasonable.

As shown in Figs. 7–9, the mutual effect is very strong when the distance is shorter than 7.5 mm. One can imagine that the discharge will be very weak and unstable when the distance is shorter than a specific value. This is validated by the discharge images shown in Fig. 10, in which the operating voltage is 16 kV. It is clear that not only does the discharge intensity of one needle become very weak and differ from the other, the discharge trajectory is also altered to be curved and unstable, particularly when the distance is 2.5 mm. Electrostatic simulation has the capability to predict this phenomenon. In the case when AR is so small that the discharge power must be very low, $E_{\max}$ is not much higher than the electric field in the vicinity that it is not capable to keep the stability.

The results of modeling and experiments (Figs. 7–10) are similar that they are mutually authenticated. Therefore, it can be concluded that electrostatic field simulation on MP barrier discharge is valid to reveal the mutual effect of nearby needles, and hence, this method can be utilized on the structure optimization of an MP reactor, particularly for the interneedle distance.

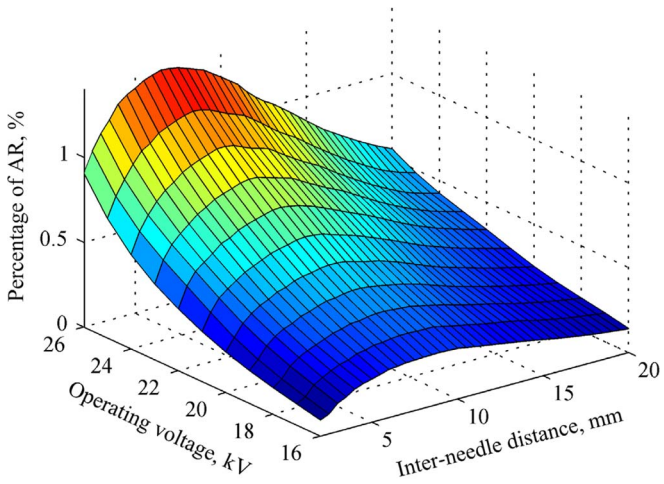

Fig. 11. Volume ratio of AR in MP barrier discharge as a function of operating voltage and interneedle distance.

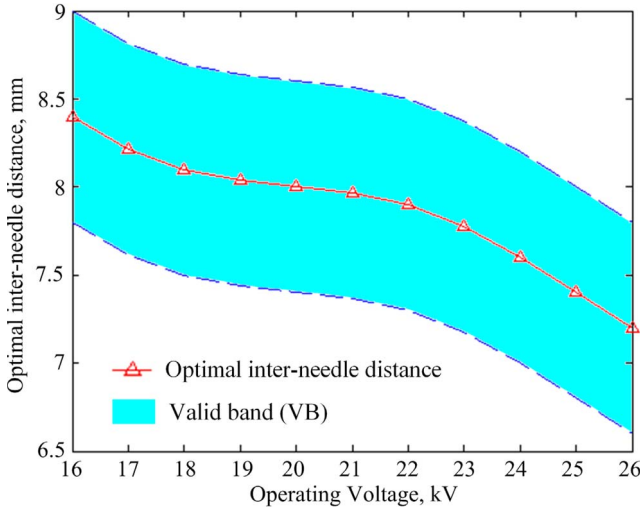

Fig. 12. Optimal interneedle distance and its corresponding VB as a function of operating voltage.

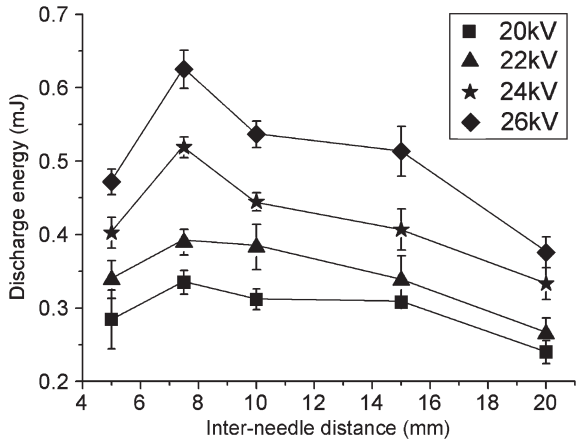

Fig. 13. Discharge energy per voltage pulse as a function of interneedle distance.

V. Interneedle-Distance Optimization

For the application of air pollution control, it is appreciated to get an appropriate discharge power density via the lowest possible operating voltage, for in that case, the cost of power supply is lowest and the security of the facility is improved. In other words, the optimal reactor structure is the structure in which, with a specific operating voltage, the maximum discharge power density can be obtained. Although the discharge intensity per needle is increasing as interneedle distance lengthens (see Section IV), this does not apply to the discharge power density of the entire reactor, because the number density of needles is decreasing simultaneously. As discussed previously, the volume ratio of AR per total air region in the reactor is a positive function of discharge power density, because the enlargement of AR will result in increased microdischarge probability. Therefore, the maximal volume ratio of AR is eventually the factor that needs to be obtained for interneedle-distance optimization.

The volume ratios of AR derived by ANSYS are shown in Fig. 11, in which the operating voltages are between 16 and 26 kV with a resolution of 1 kV and the interneedle distances are between 2 and 20 mm with a resolution of 0.5 mm. For the large scale of operating voltages, it can be seen that the volume ratio of AR always reaches its maximum when the interneedle distance is about 7.5 mm, which means that the optimal distances are all close to 7.5 mm. This optimal distance value, as well as its little change for different operating voltages, has been roughly predicted by experiments (see Fig. 8). It can be seen in Fig. 8 that the ratio of luminous to dark regions reaches its maximum when the interneedle distance is 7.5 mm.

In order to get the optimal distance value accurately as a function of operating voltage, the electrostatic field simulation is further utilized on distances between 6 and 10 mm, with a resolution of 0.1 mm. For the sake of commercial use, maybe, it is not necessary to get the optimal distance in such high accuracy, e.g., 0.1 mm. Given that the volume ratio of AR in VB is more than 99% of maximum, a distance in VB that is enough for less rigorous cases is chosen. The optimal distance and the corresponding VB are shown in Fig. 12 as a function of operating voltage. It can be seen that the optimal interneedle distance is decreasing from 8.4 to 7.2 mm when the operating voltage increases from 16 to 26 kV and the width of VB is decreasing a little from 1.2 to 1 mm. The discharges are intensified with the increase of operating voltage; thus, the mutual effect of nearby needles relatively gets weaker, and that is the reason why the optimal distance decreases.

The optimal distance and the VB in Fig. 12 are valuable for the structure presented in this paper (see the following experimental validation). If the other structural parameters change, e.g., the gap changes to be 5 mm, then the optimal distance will also change. However, the method presented in this paper is capable for optimizing not only interneedle distance but also other kinds of geometry parameters like the gap of electrodes. Also, in less rigorous cases, a rough electrostatic simulation is suitable because the VB is found to be wider than 1 mm, and therefore, the simulation becomes much easier and time saving.

The total discharge energy of the reactor per voltage pulse is shown in Fig. 13 as a function of the interneedle distance. For each case of operating voltage and interneedle distance, measurements are repeated 25 times. It can be seen that the

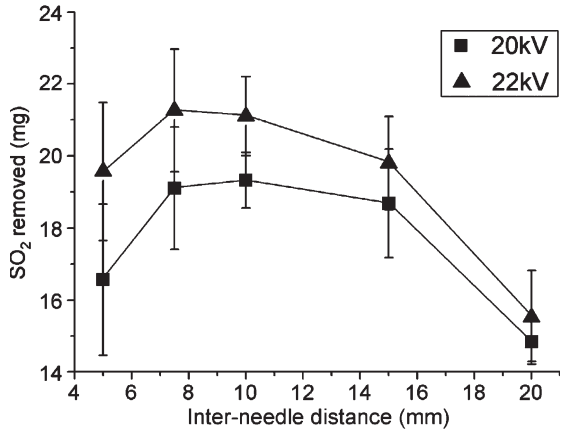

Fig. 14. SO_2 removal performance as a function of interneedle distance.

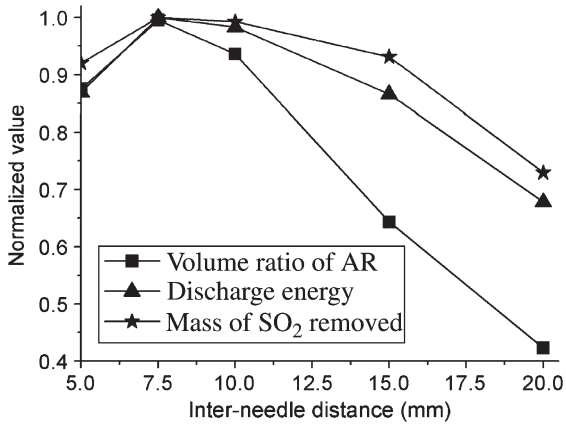

Fig. 15. Normalized value of simulation and experimental results as a function of interneedle distance.

optimal distances for discharge energy input efficiency are all close to 7.5 mm. Also, the optimal distance tends to be shorter as operating voltage increases. The experimental results are in accordance with the simulation results.

The discharge reactor is utilized to remove SO_2 from indoor air (see Fig. 6 for the air purification facility), and the performance (mass of SO_2 removed in 10 min) is shown in Fig. 14, as a function of the interneedle distance. For each case of operating voltage and interneedle distance, experiments are repeated ten times. Although the uncertainty of the experimental results are relatively high, the optimal distances at 20 and 22 kV for SO_2 removal are undoubtedly close to 7.5 mm, which is also similar to the simulation results.

In order to make the comparison of simulation and experimental results quantitatively, the volume ratio of AR, the discharge energy per voltage pulse, and the mass of SO_2 removed in 10 min are normalized and shown in Fig. 15 in the case of an operating voltage at 22 kV. The tendencies are similar with the interneedle distance as a parameter. However, when the interneedle distance is larger than 7.5 mm, the simulation result (volume ratio of AR) decreases more sharply. This is attributed to the increase of average electric field intensity in AR with the interneedle distance. In AR, the $E_{\max}$ increases (see Fig. 9) while $E_{\min} = 26$ kV/cm with the interneedle distance; thus, it is certain that the average electric field intensity increases. In order to better evaluate the energy input efficiency by modeling, the average electric field intensity in AR should be adopted as a modifying factor. However, the effect of this factor is difficult to be quantified. In a further study, we will try to take it into account.

With the discharge images, discharge energies per voltage pulse, as well as the performances on SO_2 removal, it is validated that the electrostatic field simulation has the capability, although not very accurate, to reveal the mutual effect of nearby needles and hence optimize the interneedle distance for maximum energy input efficiency.

VI. Concluding Remarks

A new structure optimization method for MP barrier discharge, particularly the interneedle distance, has been brought forward in this paper. Using electrostatic simulation, this method provides a simple way to predict the mutual effect of nearby needles on the discharge energy input efficiency and hence finds out the optimal interneedle distance as a function of operating voltage as well.

The optimal interneedle distance is found to be between 7.2 and 8.4 mm, increasing when the operating voltage reduces from 26 to 16 kV. Also, the VB is obtained with a width of not less than 1 mm. The simulation results are experimentally validated by discharge image analysis, discharge energy measurement, as well as SO_2 removal performances from indoor air. It is noted that these optimal values are only valid for MP geometries with the same needle shape and electrode separation as presented in this paper. However, the structure optimization method is validated, and therefore, the optimal interneedle distance is easy to be acquired for most cases of MP geometries.

This method leads a simple way for the optimization of interneedle distance. Furthermore, it can be used for some other structural parameters in an MP barrier discharge reactor, such as the gap between the needle and the plane electrode, the needles' shape, and so on; it is even possible to be transformed into other kinds of discharge, such as corona discharges, plasma jet matrices, etc. It is a convenient and low-cost way for structure optimization of low-frequency and low-power-density discharges.

References

[1] U. Kogelschatz, "Filamentary, patterned, and diffuse barrier discharges," *IEEE Trans. Plasma Sci.*, vol. 30, no. 4, pp. 1400–1408, Aug. 2002.

[2] K. Takaki, M. Shimizu, S. Mukaigawa, and T. Fujiwara, "Effect of electrode shape in dielectric barrier discharge plasma reactor for NO_x removal," *IEEE Trans. Plasma Sci.*, vol. 32, no. 1, pp. 32–38, Feb. 2004.

[3] F. Daou, A. Vincent, and J. Amouroux, "Point and multipoint to plane barrier discharge process for removal of NO_x from engine exhaust gases: Understanding of the reactional mechanism by isotopic labeling," *Plasma Chem. Plasma Process.*, vol. 23, no. 2, pp. 309–325, Jun. 2003.

[4] K. Takaki, M. A. Jani, and T. Fujiwara, "Removal of nitric oxide in flue gases by multipoint to plane dielectric barrier discharge," *IEEE Trans. Plasma Sci.*, vol. 27, no. 4, pp. 1137–1145, Aug. 1999.

[5] S. Futamura, H. Einaga, and A. Zhang, "Comparison of reactor performance in the nonthermal plasma chemical processing of hazardous air pollutants," *IEEE Trans. Ind. Appl.*, vol. 37, no. 4, pp. 978–985, Jul./Aug. 2001.

[6] B. M. Penetrante, M. C. Hsiao, B. T. Merritt, G. E. Vogtlin, and P. H. Wallman, "Comparison of electrical discharge techniques for nonthermal plasma processing of NO in N_2," *IEEE Trans. Plasma Sci.*, vol. 23, no. 4, pp. 679–687, Aug. 1995.

[7] A. B. Saveliev, G. J. Pietsch, A. R. Murtazin, and A. Fried, " SO_2 removal from air with dielectric barrier discharges," *Plasma Sources Sci. Technol.*, vol. 16, no. 3, pp. 454–469, Aug. 2007.
[8] X. J. Xu and D. C. Zhu, *Gas Discharge Physics*. Shanghai, China: Fudan Univ. Publisher, 1996.
[9] B. Eliasson and U. Kogelschatz, "Modeling and applications of silent discharge plasmas," *IEEE Trans. Plasma Sci.*, vol. 19, no. 2, pp. 309–323, Apr. 1991.
[10] Y. Sakiyama and D. B. Graves, "Finite element analysis of an atmospheric pressure RF-excited plasma needle," *J. Phys. D, Appl. Phys.*, vol. 39, no. 16, pp. 3451–3456, Aug. 2006.
[11] M. Rong, J. Liu, X. Wang, and X. Yuan, "Research on air purification efficiency by nonthermal plasma along with the application of magnetic field," *IEEE Trans. Plasma Sci.*, vol. 34, no. 4, pp. 1345–1350, Aug. 2006.
[12] G. E. Georghiou, R. Morrow, and A. C. Metaxas, "Characterization of point-plane corona in air at radio frequency using a FE-FCT method," *J. Phys. D, Appl. Phys.*, vol. 32, no. 17, pp. 2204–2218, Sep. 1999.

Mingzhe Rong (M'98) was born in Shanxi Province, China, on October 8, 1963. He received the B.Sc. and Ph.D. degrees from the Department of Electrical Engineering, Xi'an Jiaotong University, Xi'an, China, in 1984 and 1990, respectively.

He is currently a Professor with Xi'an Jiaotong University. Since 1984, over 160 of his papers have been published. He has been involved in arc physics, electrical contact theory, and condition monitoring techniques for switchgears.

He is a member of IEICE and China Electrotechnical Society.

Dingxin Liu was born in Chongqing City, China, on April 29, 1982. He received the B.S. degree from Xi'an Jiaotong University, Xi'an, China, in 2004, where he is currently working toward the Ph.D. degree and is involved in the simulation and diagnostics of cold plasmas. He has studied at Loughborough University, U.K., as a Visiting Student from October 2008 to September 2009.

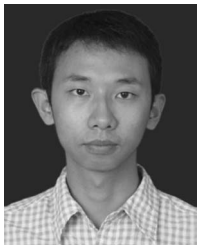

Dong Wang was born in Shaanxi Province, China, on January 23, 1985. He received the B.S. degree from Xi'an Jiaotong University, Xi'an, China, in 2007, where he is currently working toward the M.S. degree in electrical engineering.

He is currently involved in simulations of dielectric barrier discharges.

Biao Su was born in Shandong Province, China, on August 23, 1983. He received the B.S. and M.S. degrees from Xi'an Jiaotong University, Xi'an, China, in 2006 and 2009, respectively.

He is currently an Engineer with Beijing Electric Power Company.

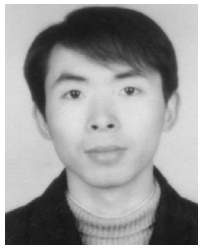

Xiaohua Wang was born in Zhejiang Province, China, on February 21, 1978. He received the B.S. degree from Chang An University, in 2000 and the Ph.D. degree from Xi'an Jiaotong University, Xi'an, in 2006.

He is currently an Associate Professor with Xi'an Jiaotong University. He has been involved in the simulation and analysis of circuit breakers, condition-monitoring techniques and fault diagnosis for switchgears, and environment protection electrical apparatus.

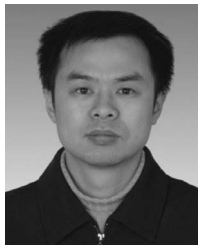

Yi Wu was born in Jiangsu Province, China, in 1975. He received the B.S. and Ph.D. degrees from Xi'an Jiaotong University, Xi'an, China, in 1998 and 2006, respectively.

He is currently with the State Key Laboratory of Electrical Insulation and Power Equipment, Xi'an Jiaotong University. His research interests include the application of fast current limiters, HTS, the electric arc phenomenon, and the analysis of the low-voltage switching devices.